The opal-CT nanostructure.

François Fröhlich

Journal of Non-Crystalline Solids 533 (2020) 119938

Contents lists available at ScienceDirect

Journal of Non-Crystalline Solids

journal homepage: www.elsevier.com/locate/jnoncrysol

The opal-CT nanostructure

François Fröhlich

Muséum national d'Histoire naturelle – Sorbonne universités, CNRS UMR 7194, Musée de l'Homme, palais de Chaillot - 17, place du Trocadéro, 75116 Paris, France

ARTICLE INFO

Keywords:
Non-crystalline silica
Tridymite structures
Infrared spectroscopy
Electron diffraction
Crystal growth

ABSTRACT

Opal-CT, a silica polymorph in marine sedimentary siliceous rocks, exhibits commonly a form of spheres about ten micrometers in diameter ("lepispheres"). Quantitative infrared analyses were performed with a special attention to the band related to the Si—O—Si angle and to the [SiO_4] tetrahedral framework. Opal-CT includes about 40% non-crystalline structures mixed with crystalline ones related to tridymite. Under TEM a single opal-CT lepisphere section exhibits a nanostructure constituted of a stacking of domains 1.5 nm thick, alternatively crystalline and non-crystalline. The crystalline domains match with a monoclinic form of tridymite which pass to non-crystalline domains with a distortion of the Si—O—Si angle. The regular stacking of crystallites 1.5 nm thick composed with about three tridymite modules is assigned to a tridymite superstructure. The paradoxical crystallization at sea water temperature of a high temperature mineral is here explained by the polymerization of silica dimers from sea water enriched with dissolved silica. Opal-CT hydrothermal in origin differs from the sedimentary one by its infrared spectrum and its optical properties that matches with the silica polymorph lussatite. It is inferred that the hydrothermal opal-CT exhibits a structure significantly different from the sedimentary one (pseudo-orthorhombic, even orthorhombic).

1. Introduction

Opal-CT is a common silica polymorph from the Cretaceous and lower Cenozoic sedimentary silicifications in the whole world. It is an important mineral in the understanding the mechanisms of formation for sedimentary siliceous rocks, and then for the reconstruction of paleoenvironments. According to the classical model of the siliceous diagenesis, it is recognized as an intermediate phase between amorphous, biogenic silica and chalcedony (e.g., see [1–3]). In another model opal-CT would originate from a direct crystallization from dissolved silica in seawater [4,5]. Therefore a precise knowledge of the nature and the structure of opal-CT is necessary to understand the mechanisms of sedimentary silicifications formation. The opal-CT structure was first described on the basis of the interpretation of X-Ray Diffraction (XRD) pattern, as low-temperature disordered cristobalite with intergrowth of tridymite layers [6–9]. This silica polymorph was labeled opal-CT (opal-cristobalite-tridymite) [7]. The XRD pattern exhibits three broad peaks near 4.30 Å, 4.10 Å and 2.50 Å (Fig. 1). Now cristobalite and tridymite are high temperature silica polymorphs crystallizing at temperatures >1000 °C, and which structure changes when cooling (e.g. see [10]), whereas whatever the genetic model, opal-CT crystallizes at sea water temperature. Thus crystallization of cristobalite and/or tridymite, high temperature minerals, at such a low temperature is paradoxical: only α quartz, the silica polymorph stable at this temperature range, would crystallize.

Moreover chalcedony, the microcrystalline form of quartz, is the main silica phase in silicified sediments, e.g. in the form of flints. Similarly opal-CT is the main constituent of cherts, common silicified rocks, where under petrographic microscope it appears as massive, opaque and without any structure, excepted within microcavities where it is often found in the form of small spheres regularly 10–12 μm in diameter, so-called lepispheres (Fig. 2). A previous study [4] made by transmitted electron microscope (TEM), electron diffraction (ED) and by infrared spectroscopy was carried out with crushed opal-CT cherts coming from Paris basin and from Atlantic and Indian oceans drilled during the Deep Sea Drilling Project (D.S.D.P.) in the seventies. In this previous study, the ED patterns low resolution, caused by structural changes of opal-CT resulting from heating under the electron beam [11,12] have failed to distinguish 4.10 Å reflection of both cristobalite and tridymite from tridymite 4.30 Å one. According to the dark field images [4], the sedimentary opal-CT structure consists in nanophases, alternating diffracting and non-diffracting domains of 5 nm thick and 50 nm width. Thus the model of intergrowth cristobalite-tridymite proposed by Flörke [6] could not be confirmed. The same specimens showed the absence of lattice vibration modes (especially cristobalite ones) on opal-CT infrared spectra [4,13] and then led to the same conclusion.

For this reason it was necessarily to refine the opal-CT

E-mail address: frohlich@mnhn.fr.

https://doi.org/10.1016/j.jnoncrysol.2020.119938
Received 26 September 2019; Received in revised form 6 January 2020; Accepted 15 January 2020

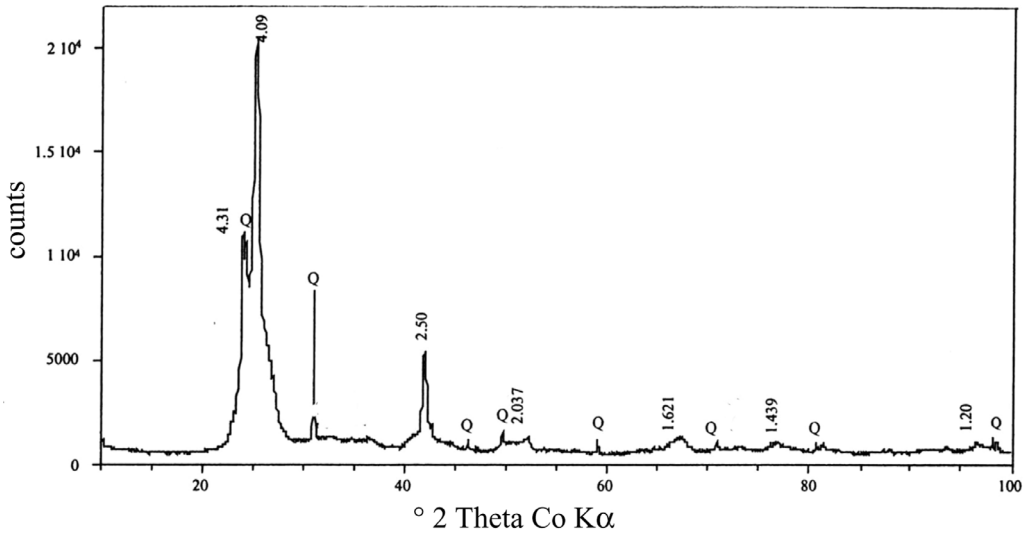

Fig. 1. Bulk Baudres lepispheres deposit. Co Kα X-ray diffraction pattern. *Q* = quartz.

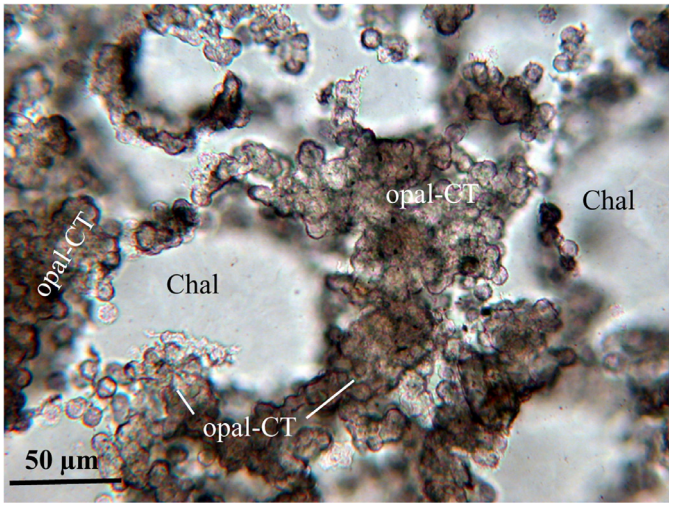

Fig. 2. Thin section, parallel polars, of a middle turonian chert drilled at Civray-de-Touraine (Indre et Loire, France). MNHN collections. Chal = chalcedony.

nanostructure, which appears well expressed in lepispheres. This paper is aimed to present new TEM data carried out from single lepispheres, to refine the IR data and to determine the potential differences between opal-CT sedimentary and hydrothermal in origin, presenting an opal-CT X-ray pattern [14,15].

2. Materials

The sedimentary opal-CT comes from Baudres (Touraine, Paris basin, France) a soft deposit dating from the lower Turonian geological stage, 85 Million years (My) old, and constituted by the accumulation of single opal-CT lepispheres [16]. Its mineralogical composition, computed from Fourier Transform Infra Red (FTIR) analysis according to the method described below is: opal-CT, 89%; quartz: 9.5%; kaolinite (clay mineral): 1.5%.

Cristobalite was synthesized by firing chalcedony over 12 h at 1500 °C

Pure tridymite crystals were not analyzed, because of their scarcity in the nature and of significant difficulties in synthesis.

The hydrothermal opal-CT comes from a green opal of gem quality vein, in pyroclastics deposits of an Oligocene (about 30 My old) volcano in Biot (near Nice city, France). It is composed of: SiO_2 (in the form of opal-CT), 89%; Al_2O_3, 7.5% (in the form of allophanes, amorphous clay mineral); CuO, 3.0% (responsible for the green color) [14].

3. Methods

3.1. Fourier transform infrared (FTIR)

FTIR analyses were performed using the KBr pellet method adapted to quantitative analyses according to the Beer–Lambert Law [17–19]. The samples were mechanically ground using acetone in an agate cell with three small agate balls. To prevent structural changes due to heating, grinding was performed in a refrigerated area. To avoid scattering IR radiation, and then to apply the Beer–Lambert law, a particle size less than the shorter wavelength (2.5 µm) is required [20]. The grain size was verified on smear slides and under a petrographical microscope. The powdered samples were mixed with KBr in the proportion 400:1 by weight to yield a standard dilution of 0.25%. A 300 mg pellet (thus containing 0.75 mg of sample) was made by pressing the mixture in a vacuum die with up to 1000 kg cm^{-2} of compression. Weighing was performed with an accuracy of 10^{-5} g. The absorbance of each absorption band of a mineral spectrum is thus specific for a standard mass (here, 0.75 mg in a 300 mg pellet), and then make possible the determination of the minerals percentages in rocks as well as a comparison of the main IR parameters between different minerals.

The pellets were analyzed with a Bruker VERTEX 70 FTIR spectrophotometer between 4000 and 400 cm^{-1} at a 4 cm^{-1} resolution, 0.6 cm^{-1} accuracy and with an accumulation of 32 scans of 2 s each. Wavenumber data are here displayed with $a \pm 0.3\ cm^{-1}$ uncertainty.

Thanks to the analytical procedure used here, for each absorption band, four main typical spectral parameters giving good indications of the three-dimensional geometry of the [SiO_4] tetrahedra framework are taken into account:

1 The wavenumber ν (stretching vibration modes) or δ (bending vibration modes) of the absorption maximum.
2 The absorbance A (in arbitrary units), related to the quantity of elemental vibrators, is measured on the spectrum in using the empirical method of the base line [18,19]. Thanks to the standard analytical procedure used here, and according to the Beer-Lambert law, A is a linear function of the mass of the mineral analyzed [18]: $A = a.l.c$, where A is the absorbance of a band, α = the molecular extinction coefficient (a constant), l = the optical path length (here,

the pellet thickness: 0.83 mm, a constant), c = the mineral concentration (for pure minerals, c = 1). In the case of mineral mixtures, c is computed in reference to a 0.75 mg mass of pure mineral according to the MNHN standard IR data bank. The uncertainty ΔA is computed from the uncertainty of the baseline position [18,19].

3 The half-width $\Delta\nu$ (= width in cm^{-1} of the absorption band at half absorbance), related to the dispersion of the wavenumber values of a vibration mode.

4 The integrated intensity I (surface of the band, in arbitrary units), which corresponds to the sum of the total energy involved in this vibration mode. Because of the baseline position uncertainty, the I values were not obtained here with the OPUS Brucker software, but by computing A.$\Delta\nu$, a good approximation for quite pure Lorentzian/Gaussian bands, and to avoid the deformations of a band, due to weak overlapping bands.

3.2. Scanning electron microscope (SEM)

The specimens were coated with an about 20 nm thick Au/Pd layer. The soft opal-CT from Baudres was dispersed in water and a drop put on a metallic specimen holder, dried and then metalized.

3.3. Transmitted electron microscope (TEM)

The TEM analyses were carried out on a JEOL 100 CX apparatus equipped with an energy-dispersive X-ray spectrometer. Preparations of ultra-thin sections, 50 to 80 nm thick, of opal-CT lepispheres from the Baudres soft sediment were obtained by microtoming an epoxy resin block containing pulverized soft sediment, using the diamond blade of a Reichert Ultracut E ultra-microtome. In order to limit the beam damage and then amorphization or structural changes, observations were conducted under low intensity and exposure time. In these conditions [21], electron diffraction (ED) patterns, bright field and dark field images could be obtained on the same selected area. Previous data [4] were obtained from a crushed acid decalcified silicified Santonian chalk (hole GI2, Gargenville, Normandie, France [4,5,22]) and from a crushed Paleocene chert (hole D.S.D.P. 25.245, Madagascar basin, Indian ocean [4]).

4. Results

4.1. Bulk analysis. FTIR data

Like pure silica glass, both Baudres and Biot opal-CT exhibit an infrared spectrum with only three broad absorption bands (Fig. 3), typical for a three-dimensional [SiO_4] tetrahedral network. These three bands are characteristic for all the 4-coordinated silica phases, with varying wavenumbers (Table 1). Additional bands related to the crystalline network present in the standard IR spectra of quartz and cristobalite (Fig. 3) are absent in tridymite spectra (or very weakly present in some tridymites [24]). Amorphous, biogenic silica exhibits an additional band at 950 cm^{-1}, related to Si—OH bonds [19,25] (Fig. 3).

The three absorption bands include:

- *Near 1100 cm^{-1}, the main absorption band* is assigned to an internal, triply degenerated ν Si—O stretching vibration mode of the [SiO_4] tetrahedron, due to the high symmetry of this unit molecule, which exhibits a threefold axis along each Si—O bond. Then the absorbance of this band is strongly strengthened.
- *The 477 cm^{-1} band* is assigned to an internal, triply degenerated δ bending Si—O vibration mode of the [Si-O_4] tetrahedron. This wavenumber varies over a large range, according to the different silica phases (Table 1).
- *The 790–800 cm^{-1}band* is assigned to a bending δ Si—O—Si intertetrahedral vibration mode. The wavenumber of this band, which varies significantly for the different silica phases (Table 1), is a function of the mean Si-O-Si bonding angle [19]. This band position is significantly different in wavenumber for Baudres and Biot opal-CT, the later being close to the tridymite one [24,26]. As seen on Fig. 3, specific intense cristobalite bands (620 cm^{-1}, 385 cm^{-1}) are lacking on the opal-CT spectrum. This observation agrees with Wilson's [13] who deducted from different spectroscopic analyses that cristobalite was not significantly present in opal-CT structure, and that only tridymite may account for it. However the very weak bands at 540 cm^{-1} and 570 cm^{-1} on the high temperature, meteoritic tridymite [24] are neither observed on opal-CT spectra.

The four parameters for this Si—O—Si band are given on Table 2: the absorbance value is highly variable, between 0.185 (amorphous, biogenic silica), and 0.94 (quartz): the absorbance of amorphous (glass) and poorly crystallized (opal-CT) phases is strongly lowered. The lowest value seen for biogenic amorphous silica is related to the substitution of one for 4 Si—O—Si bonds by Si—OH (Si—OH band at 950 cm^{-1} [19,25]). Opal-CT does not exhibit such Si—OH bonds (Fig. 3). Likewise, the half width $\Delta\nu$ exhibits very large variations, the amorphous phases presenting the highest values, and the better crystallized phases (quartz, cristobalite), the lower values. In addition the integrated intensity I (normalized for 100% mineral) remains rather constant for all the silica phases (15.2 ± 0.6; Table 2). This indicates that the sum of the vibrating bonds between the tetrahedra is essentially identical for the studied silica and for the other silica minerals: each oxygen atom is linked to two silicon atoms. However the broadening of the absorption band indicates a large scattering of the total energy of this vibration mode. The half width is actually about half-way between quartz and silica glass values (Table 2). This is related to a scattering of the Si-O-Si angle values around the mean value. Therefore the absorbance of this band is strongly lowered in comparison to quartz or cristobalite. In the absence of other absorption bands or shoulders as seen on the second derivative spectrum, (Fig. 4), e.g. near 806 cm^{-1} (amorphous, silica glass), and considering the shape of this band is symmetrical, with a ½ $\Delta\nu$ close to 20 cm^{-1} for the Biot opal-CT and 17 cm^{-1} for the Baudres one, it appears that opal-CT is composed of a large proportion of non-crystalline network coexisting with a crystalline one

The proportion of non-crystalline material can be roughly estimated from the spectral parameters of the Si—O—Si band (Table 2). Thus the integrated intensity I, which is rather constant for all the silica phases, is the sum of those of the crystalline and non-crystalline networks. If we consider that the half-width minimum value for a perfect silica crystal is reached for quartz (15.3 cm^{-1}), then the non-crystalline contribution in this band is the total half-width minus the quartz value: 39.7 cm^{-1} to 15.3 cm^{-1} = 24.4 cm^{-1} for Biot opal-CT, and 34.0 cm^{-1} to 15.3 cm^{-1} = 18.7 cm^{-1} for Baudres opal-CT. Then the proportion of non-crystalline network in the opal-CT structure may be roughly computed with reference to the integrated intensity using the Libyan Desert Glass (LDG) and Biot opal-CT IR parameters (Table 2):

$$I(\mathrm{LDG})/I(\mathrm{total}).\ 100 = 0.25 \pm 0.006*24.4/15.6 \pm 0.18*100$$
$$= 39.10\ \% \pm 0.5\ \%$$

Concerning the Baudres opal-CT, the proportion of non-crystalline network is then of 33.10% ± 0.3. Nevertheless the non-crystalline material being not characterized by a typical silica glass structure, it is deduced that ordered and disordered domains are narrowly associated with a progressive modification of the Si-O-Si angle, the ordered domains being close to a tridymite-type lattice.

4.2. Petrographic microscope observations

Fig. 2 displays a typical chert microstructure, with opal-CT and chalcedony. Lepispheres and massy sedimentary opal-CT appear isotropic under petrographic microscope. Lepispheres constitute the framework of the chert, and chalcedony the cement. Sedimentary opal-CT

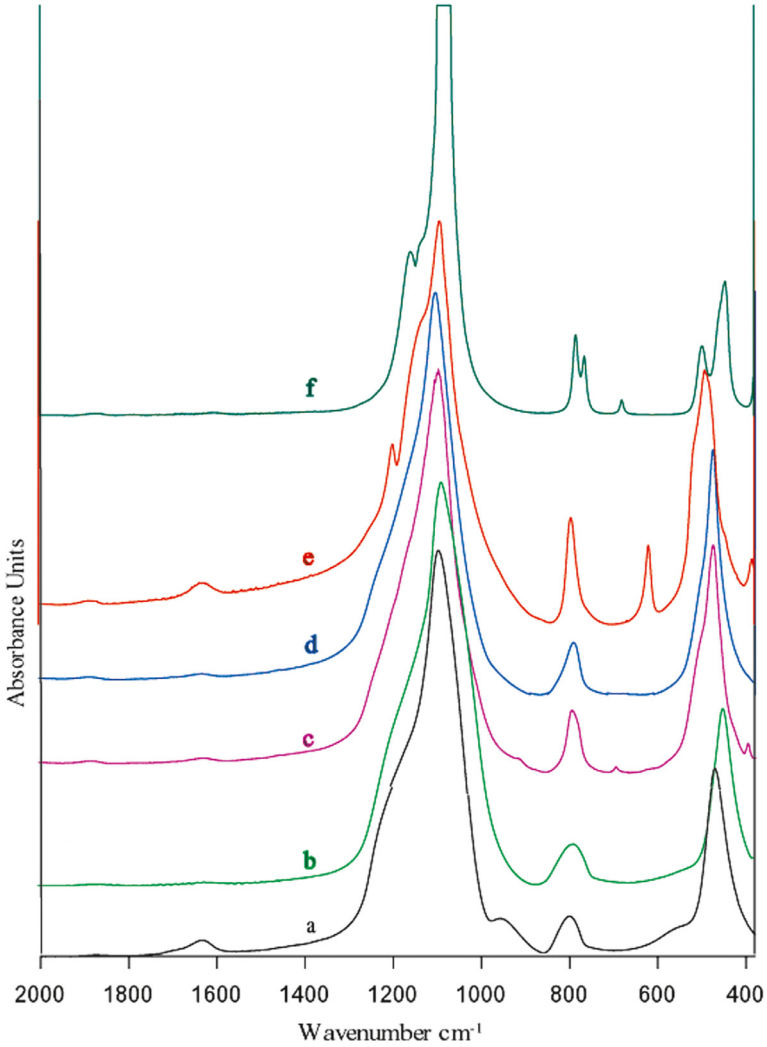

Fig. 3. Infrared spectra of different silica phases. a: sponge spicule (biogenic,amorphous silica [23]); b: pure silica glass (Libyan Desert Glass [23]); c: Baudres opal-CT; d: Biot opal-CT; e: synthetic cristobalite; f: quartz. 0.75 mg analyzed in a 300 mg KBr pellet.

Table 1
Wavenumber of the three absorption bands for different 4-coordinated silica phases. The uncertainty, ± 0.3 cm^{-1}, is a constant.

	ν Si−O	δ Si−O−Si	δ Si−O
opale-CT Biot	1103	791	475
opale-CT Baudres	1099	794	475
Libyan Desert Glass [23]	1102	806	472
opal-A biogenic silica [23]	1096	800	470
cristobalite	1089	797	487
quartz	1088	799	464

appear isotropic under petrographic microscope, but Biot opal-CT exhibits on the contrary a length-slow, fibrous radiating structure showing a low birefringence. This microfabric resembling chalcedony (Fig. 5) is typical of the silica polymorph lussatite [27,28].

4.3. Single lepisphere analyses

A powder XRD pattern of the bulk Baudres silica (Fig 1) exhibits three broad diffraction bands at 4.31, 4.09 and 2.45 Å, according with other published patterns for opal-CT. Narrow additional peaks (mainly at 4.25 Å and 3.34 Å) are related to quartz impurities. The 4.09 Å value for the main peak is closer to the 4.10 Å value reported for low-temperature tridymite than to the 4.039 value for low-temperature

Table 2
δ Si−O−Si band spectral parameters for the different silica phases. 0.75 mg analyzed in a 300 mg KBr pellet. (1): this work; (2): Fröhlich et al. [23]. The wavenumber uncertainty is ± 0.3 cm^{-1}.

	ν cm-1	**A**	Δν cm^{-1}	**I**	**I***(100%)*
opale-CT Biot(1)	791	0.35 ± 0.004	39.7	13.90 ± 0.16	15.60 ± 0.18
opale-CT Baudres (1)	794	0.38 ± 0.006	34.0	12.90 ± 0.20	14.50 ± 0.23
Libyan Desert Glass [23]	806	0.25 ± 0.006	62.0	15.50 ± 0.40	15.80 ± 0.40
opal-A biogenic silica [23]	800	0.19 ± 0.010	52.5	10.00 ± 0.50	10.00 ± 0.50
cristobalite (1)	797	0.69 ± 0.010	21.9	15.10 ± 0.22	15.10 ± 0.22
quartz (1)	799	0.94 ± 0.005	14.4	15.05 ± 0.05	15.05 ± 0..05

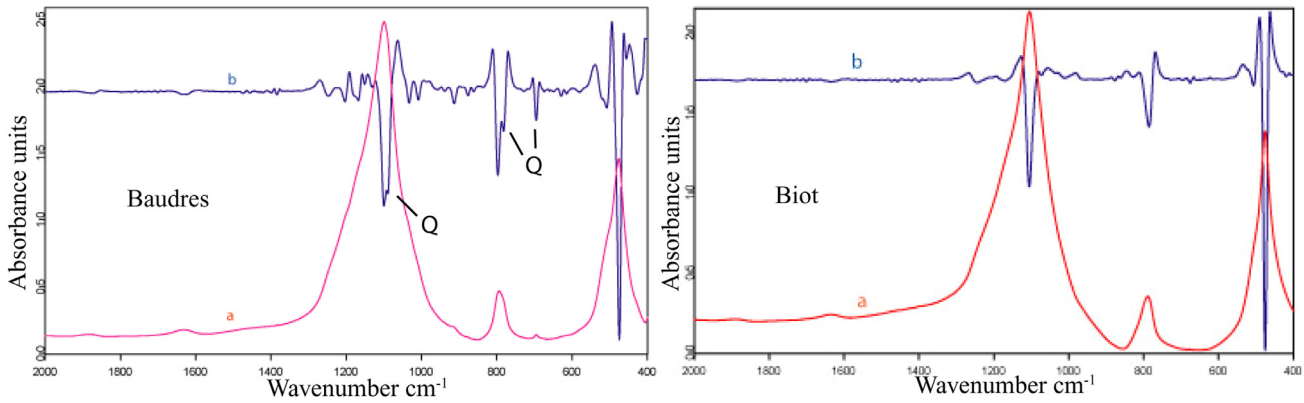

Fig. 4. Opal-CT Si—O—Si band. IR spectrum (a), and second derivative spectrum (b). Left: Baudres opal-CT (*Q* = quartz) ; right : Biot opal-CT. The second derivative spectrum highly expand the weak absorption bands of secondary constituents.

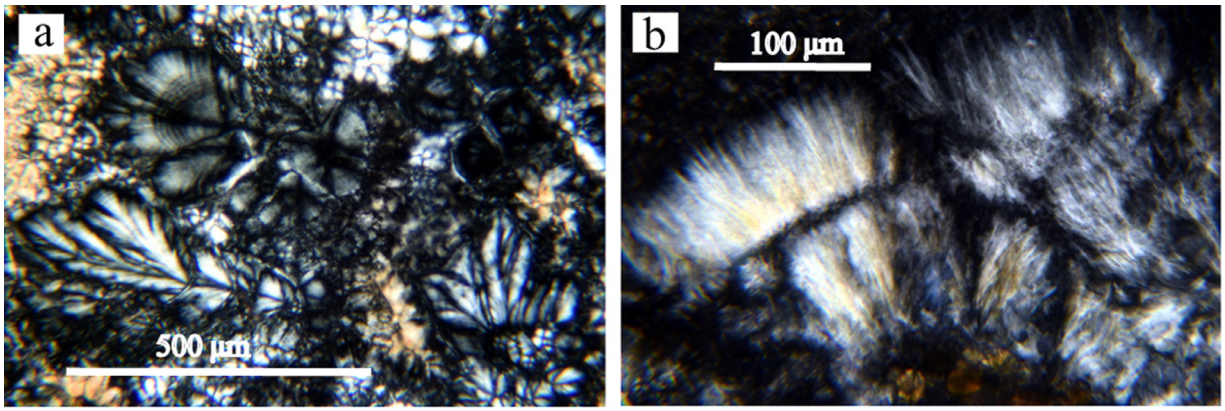

Fig. 5. Thin section of Biot opal-CT, crossed polars. (a) : the fibrous radiating matrix exhibits typical birefringence figures of lussatite. (b) : details of the fibrous structure, length-slow fibers about 80 µm long.

cristobalite [2].

4.3.1. Scanning electron microscope observations

The rather pure opal-CT soft sediment from Baudres exhibits an accumulation of lepispheres, regularly 10–12 µm in diameter. The fibrous radiating structure of lepispheres clearly appears (Fig 6a) on broken surfaces. With a higher magnification (Fig 6b), the external morphology exhibits typical intergrown thin blades, about 200 nm thick, constituted of the accumulation of nanoparticles about 50 nm wide, which appear well individualized at the lepisphere periphery.

4.3.2. Tranmission electron microsopy observations

Complete section of the Baudres lepispheres, up to 10 µm in diameter and thus almost equatorial, have been observed under TEM (Fig. 6e). This section exhibit “bundles” of elongated bodies probably related to sections of blades seen under SEM (Fig. 6a). These morphologies are more apparent and often isolated towards the outer few micrometers of the lepispheres (Fig. 6e). Both TEM and SEM observations lead to the interpretation of the blades as an assemblage of elemental rods, 10 to 15 nm width, whatever the length is. The scale-like texture of the inner part of the sections is an artifact due to ultramicrotome knife impact.

4.3.3. Electron diffraction

The ED patterns obtained on large selected areas (2.6 µm in diameter) of the lepisphere, including both peripheral and central domains, consist of discontinuous, concentric rings (Fig. 6c and f). The innermost and strongest diffraction ring exhibits six enlarged reflections that correspond to a hexagonal net (Fig. 6f). The corresponding *d*-spacing ranges between 4.10 Å to 4.30 Å, like on the XRD pattern (Fig. 1, Table 3), and the anisotropic distribution of intensity suggests preferred orientations in the selected area from which the pattern was produced. Generally speaking, the *d*-spacing measured on the ED pattern for lepisphere sections (Table 3) are in accordance with the *d*-spacing value of 4.3 Å (Fig 6f) and the *d*-spacing value for 2.5 Å (Fig. 6f) obtained on bulk Baudres silica via XRD (Fig 1; Table 3), and with those previously published for silicified chalks and cherts from the Paris basin and from oceanic basins [4] (Fig. 6c).

ED patterns from smaller selected areas (0.6 µm) have been performed on rods in the outer and inner areas of the lepisphere section. Both give diffraction patterns that consist on a central row and spots. Even selected areas of small size aggregates of thin plates give polycrystalline patterns.

4.3.4. Dark field images

Dark field images were obtained using the reflection at 4.1 Å, in order to investigate the elongated domains from which this reflection originates. Extremely thin, elongated and sub-parallel areas in diffraction orientation are separated by regions lacking reflection contrasts (Fig. 6d and h), each one being 1 to 1.5 nm thick and 10 to 20 nm long. The non-contrast areas are deduced to derive from structural disorder due to the lack of correlated diffraction. At the periphery of the lepisphere sections, it was observed that some blades sections display dark field images with more continuous and massive domains due to the 4.1 Å diffraction. This feature reveals a better crystalline organization at the margin of the lepisphere.

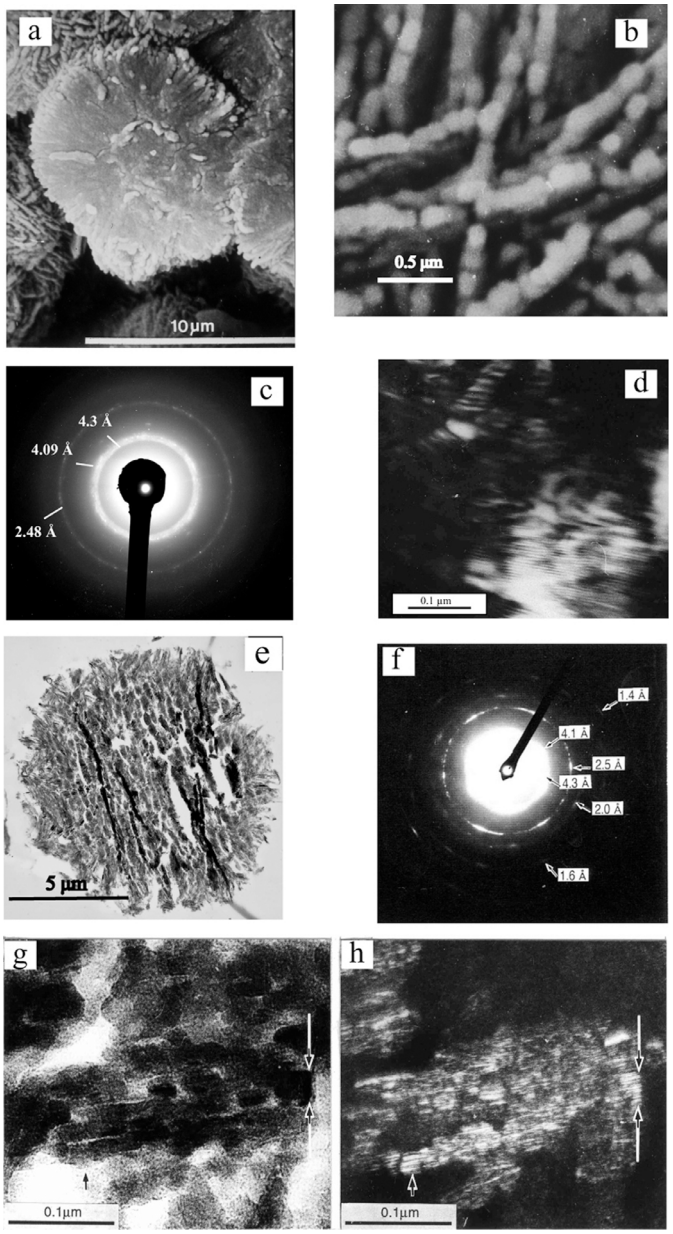

Fig. 6. (a): SEM image of Baudres lepisphes. The broken lepispheres exhibit a fibrous radiating structure, well expressed outwards. (b): detail of a lepisphere surface. (c): ED of a crushed chert from the Indian ocean (hole D.S.D.P. 25.245.7.cc. (d): dark field image of the same sample, at a higher magnification. (e): TEM image of an equatorial ultra-thin section of a lepisphere from Baudres. (f): ED carried out on a 2.6 µm large area from (e) section. g: bright field image of the inner part of the lepisphere section; bundles are arrowed. (h): corresponding 4.1 Å dark field image.

5. Discussion

Table 3 displays a good correlation between the bulk structural data (XRD) and the small-scale structural data performed on single lepispheres (ED). The lepispheres appear to be constituted of blades, themselves composed of coalescent rods. The bulk lepisphere section ED patterns corresponds to the single rod ones. Dark field images of small domains provide additional information. The rods and the blades constituting the lepisphere are both polycrystalline (dark field, Fig. 6g and h). The non-diffracting material between the crystallites is believed to be related to the non-crystalline structures identified on the IR spectrum, a progressive ordering of the silica material leading to crystallites with tridymite-like structures.

The structure of low temperature tridymite was described from single crystals (e.g., meteoritic in origin) which result from the quenching of high temperature tridymite [10,11,24,30–34]. The highly complex structure of tridymite consists of the stacking sequence along the *c* axis of silica sheets of six members rings of [SiO_4] tetrahedra pointing alternatively up and down [24]. Therefore the unit module of all the tridymite structures is typically a two layers unit. The symmetry of this stacking module and of the unit rings strongly depends on temperature [10,12,24,29,30,33]. At high temperatures (>380 °C), Tridymite exhibits a hexagonal network (HP-tridymite [29]). With lowering temperature, the structure changes: between 380 °C and 110 °C, tridymite is orthorhombic and finally becomes monoclinic below 110 °C (MC-tridymite or PO-tridymite, pseudo-orthorhombic, cf. [10]), even at a lower temperature (below 65 °C [24,33]). The orthorhombic and monoclinic structures result in the lowering of symmetry and then in a heterogeneity of tetrahedral rings along rows within each layer, alternating ditrigonal (2/3) and oval (1/3) in shape [10]. This variability in the [SiO_4] rings shape leads to a variation of the Si-O-Si angle, and then to a significant shift in wavenumber for the related band [35].

Such structures were defined by cooling high temperatures tridymite single crystals, meteoritic, volcanic in origin, or synthesized at high temperature, proceeding from the crystallization of a silicate melt. Now opal-CT does not result from cooling high temperature crystals, but from a direct crystallization in silica-rich sea water at room temperature [14,16], or from hydrothermal dissolved silica in volcanoes environments. Dissolved silica is present at low concentration in the monomer H_4SiO_4 state. At higher concentrations, percent of the dimer $Si_2O(OH)_6$ quickly increases, up to 40% at 110 ppm, silica saturation in pure water [34], a value strongly lowered down to 31 ppm in sea water [37]. Then we can infer that in such conditions, polymerization of dimers leads to the crystallization of two layers tridymite modules, in place of quartz which crystallizes from monomer silica at lower silica concentrations [5]. Cristobalite, which structure consists of the stacking of three layers modules (e.g., see [10,36]) cannot be involved in such a process.

TEM dark field images exhibit crystallized domains about 1.5 nm thick, alternating with non-crystallized domains of a rather equivalent thickness. This is consistent with experimental studies on SiO_2 nanophases, which shows an initial nucleation of particles 1.4 nm in diameter [38]. Overall the opal-CT unit particles (crystalline + non-diffracting), up to 3 nm thick, may include only six tridymite-like modules.

Table 3
XRD and ED data. (1): Baudres, this work; (2): crushed acid leached silicified chalks from Gargenville, D.S.D.P. holes 25.245 (Madagascar basin, Indian ocean) and 3.22 (southern Atlantic ocean) [4]; (3): Fröhlich et al. [14]; (4): Cady et al. [2].

XRD Baudres (1)	Previous data (2)	Biot (3)	MC Tridymite (4)	PO Tridymite (4)	α-cristobalite (4)	ED Baudres (1)	previous data (2)
4.31	4.3	4.3	4.32	4.3	_	4.3	4.3
4.09	4.09	4.11	4.09	4,09	4.05	4.1	4.07
2.5	2.48	2.5	2.5	2,48	2.49	2.5	2,.48

To minimize the repulsion between basal oxygen atoms [10] the tilting of opposite tetrahedra within the elemental monoclinic (or pseudo-orthorhombic) tridymite module induces a progressive distortion of the Si-O-Si angle between the successive modules. This stacking disorder would be analogous to the so-called turbostratic stacking in the clay minerals smectites [39]. So, during the particles grow the stacking of tridymite modules losts quickly the overall symmetry. Monoclinic and pseudo-orthorhombic tridymite may often exhibit superstructures with a limit of the tridymite modules number [29]. We infer that the regular alternating nano domains diffracting/non-diffracting, constituted with about six tridymite-like modules along the rods in opal-CT lepispheres may therefore be considered as a tridymite superstructure. Then according to [40] opal-CT "would be accurately described as a "disordered tridymite" phase".

Finally the hydrothermal Biot opal-CT exhibits an IR spectrum slightly different from the sedimentary Baudres one. As seen on Table 2 the Si-O-Si band, which wavenumber is a function of the Si-O-Si angle, is 794 cm^{-1} for Baudres and 791cm^{-1} for Biot, a value close to that of tridymite standard [24,26,35], high temperature in origin. The transition between the orthorhombic structure and the monoclinic one between 65 °C and 110 °C is not clear, implies a collapse of the structure with modifications of the Si-O-Si angle in the range 143.2°−156° [29] and then a variation of the wavenumber of the related band, when the Si-O-Si angle is 146° for sedimentary opal-CT [30]. The sequence of phase transition and temperatures is not clear, strongly depending on the thermal history and may include incommensurate transitional phases [24]. Sedimentary opal-CT crystallizes at a temperature far below 110 °C, and then with a MC monoclinic structure [29]. Biot hydrothermal opal-CT which crystallizes at a temperature > 110 °C, and then initially with an orthorhombic structure, undergoes a critical structural change when cooled at room temperature, becomes monoclinic but exhibits a Si-O-Si angle slightly higher than sedimentary one (thus close to 148° with reference to the empirical relationship [19]). This would indicate that Biot hydrothermal opal-CT has then acquired a structure significantly different from opal-CT crystallized at sea water temperature. Considering the specific optical properties of Biot opal-CT (lussatite, labeled opal-CT_L [28]), its birefringence can be explained by a pseudo-orthorhombic (PO) symmetry, or even orthorhombic (OP [23], considering the large hysteresis of tridymite when cooling [29]). PO tridymite usually exhibits super symmetries consisting in the repetition of a given number (n) of stacking modules (tridymite POn, [11]). Such a superstructure implies crystallites constituted by a number of modules higher than sedimentary opal-CT ones and then with a greater thickness. The more important size of the crystallites and the pseudo-orthorhombic, or even orthorhombic structure, may account for the birefringence and for the special figures seen under petrographic microscope.

6. Conclusion

Sedimentary opal-CT exhibits a structure of nanoparticles about 3 nm thick. The particular characteristics of FTIR, XRD and ED patterns lead to assign this structure to a monoclinic, tridymite phase, every particle being constituted with a well crystallized tridymite domain passing to a non-crystalline one through a modification of the Si-O-Si angle. This structure is well expressed in lepispheres, exhibiting a fibrous, radiating structure with rods constituted with the regular stacking of such nanoparticles. Thus this nanophase structure of sedimentary opal-CT may be interpreted as a tridymite superstructure. The formation of tridymite at sea water temperature is related to the special behavior of silica in solution: the dimers percentage increases with silica concentration and then leads to their polymerization with the crystallization of two layers tridymite unit modules. The opal-CT crystal growth is greatly made easier in sea water.

Biot hydrothermal opal-CT exhibiting specific optical and IR properties, matches to the so-called fibrous silica polymorph lussatite. This specificity, inherited from its thermal history, correspond to a different structure than sedimentary opal-CT, probably pseudo-orthorhombic. The fibrous, lussatite form seems to be typical of hydrothermal opal-CT. Then the presence of lussatite in siliceous rocks is an indication of a hydrothermal environment.

Declaration of Competing Interest

None.

Acknowledgements

This work was supported by the Centre National de la Recherche Scientifique (CNRS) and specifically by UMR 7194. The author thanks the National Museum of Natural History (MNHN) and the Association of Geologists of the Paris Basin (AGBP) for the permission to reproduce figures. The author thanks Denise Badaut for assistance and providing TEM data, Tassadit Nait for cristobalite synthesis, Xavier Gallet for laboratory facilities, Patrick Schmidt for refining references.

The author especially thanks Christine Fröhlich for improving the English language, Catherine Mignaud, Pierre-Jacques Chiappero and Matthieu Lebon for their attentive reading, their judicious remarks and the improvement of this paper.

References

[1] L.P. Knauth, Petrogenesis of chert, Silica, physical behavior, geochemistry and materials applications, in: P.J. Heany, C.T. Prewitt, G.V. Gibbs (Eds.), Eds, Silica Physical Behavior, Geochemistry and Materials Applications, 29 1994, pp. 233–258 Rev. in Min.Miner. Soc. Amer. Washington.
[2] S.L. Cady, H.-R. Wenk, K.H. Dowing, HRTEM of microcrystalline opal in chert and porcelanite from the Monterey Formation, California, Amer. Miner 81 (1996) 1380–1395.
[3] M. Liesegang, R. Mielke, C. Berthold, Amorphous silica maturation in chemically weathered clastic sediments, Sedim. Geol. 365 (2018) 54–61, https://doi.org/10.1016/j.sedgeo.2018.01.001.
[4] F. Fröhlich, Les silicates dans l'environnement pélagique de l'océan Indien au Cénozoïque, Mém. Mus. Nat. Hist. Nat., Nelle Sér. C. tome XLVI (1981).
[5] F. Fröhlich, Silex et cherts : questions de genèse, Bull. Inf. Ass. Géol. Bass. Paris. 43 (2) (2006) 5–22 n.
[6] O.W. Flörke, Zur Frage des « Hoch »-Cristobalit in Opalen, Bentoninen and Gläsern, Neu Jb. Min. Mon (1955) 217–223.
[7] J.B. Jones, E.R. Segnit, The nature o f opal. Nomenclature and constituent phases, J. Geol. Soc. Australia 18 (1971) 57–68.
[8] O.W. Flörke, H. Graetsch, B. Martin, K. Röller, R. Wirth, Nomenclature of micro- and non-crystalline silica minerals, based on structure and microstructure, Neu Jb. Min. Abh 163 (1) (1991) 19–42.
[9] H. Graetsch, H. Gies, I. Topalovic, NMR, XRD and IR study on microcrystalline opals, Phy. Chem. Minerals 21 (1994) 166–175.
[10] PJ Heany, Structure and chemistry of low pressure silica polymorphs, in: P.J. Heany, C.T. Prewitt, G.V. Gibbs (Eds.), Silica Physical Behavior, Geochemistry And Materials Applications, 29 1994, pp. 1–40 Rev. in MinMiner. Soc. Amer. Washington.
[11] M.A. Carpenter, M. Wennemer, Characterization of synthetic tridymite by transmission electron microscopy, Amer. Miner 70 (1985) 517–528.
[12] J.R. Ashworth, Transmission electron microscopy of coexisting low-tridymite polymorphs, Miner. Mag 53 (1989) 89–97.
[13] M.J. Wilson, The structure of opal-CT revisited, J. non-Cr. Solids 405 (2014) 68–75, https://doi.org/10.1016/j.jnoncrysol.2014.08.052.
[14] F. Fröhlich, Mari G., D. Mari, Les silicifications hydrothermales à opale de Biot (Alpes-Maritimes), Le règne Minéral 40 (2001) 5–12.
[15] M. Hatipoglu, Y. Kibici, G. Yanik, C Ozkul, M. Demirbilek, Y. Yardimci, Nanostructure of the cristobalite and tridymite stacking sequences in the common Purple Opal from the Gevrekseyidi Deposit, Seyitömer-Kütahya, Turkey, Orient. Journ. Chem 31 (1) (2015) 35–49, https://doi.org/10.13005/ojc/310104.
[16] S. Mouhsine, Processus de la silicification sédimentaire ; Modèle du Turonien de Touraine, Thèse Mus. Nat. Hist. Nat., Paris (1994).
[17] F. Fröhlich, L. Leclaire, L'analyse des sédiments pélagiques associés aux nodules polymétalliques par la spectrométrie d'absorption infrarouge, Bull. Mus. Nat. Hist. Nat. 4ème sér. 3 C n°1, Paris (1981) 159–181.
[18] C. Pichard, F. Fröhlich, Analyses IR quantitatives des sédiments, Exemple du dosage du quartz et de la calcite, Rev. Inst. Fr. Pétrole 41 (6) (1986) 809–819, https://doi.org/10.2516/ogst:1986048.
[19] F. Fröhlich, Biogenic silica, new structural and analytical data from infrared analysis – geological implications, Terra Nova 1 (1989) 267–273, https://doi.org/10.1111/j.1365-3121.1989.tb00368.x.
[20] G. Duykaerts, The infrared analysis of solid substances, Analyst 84 (1959) 201–214.
[21] D. Badaut, F. Risacher, Authigenic smectites on diatom frustules in Bolivian saline

lakes, Geoch. Cosmoch. Acta 47 (1983) 363–375, https://doi.org/10.1016/0016-7037(83)90259-4.
[22] F. Fröhlich, Le Sénonien de, l'ouvrage souterrain de Gargenville, in: J.P. Gély, F. Hanot (Edit.), Le Bassin Parisien, Un nouveau regard sur la géologie, Assoc. Géol. Bass, Paris, Paris, 2014, p. 201.
[23] F. Fröhlich, G. Poupeau, A. Badou, F.-X. Le Bourdonnec, Y. Sacquin, S. Dubernet, J.-M. Bardintzeff, M. Véran, D.C. Smith, E. Diemer, Libyan Desert Glass: new field and Fourier Transform Infrared Data, Meteorit. Planet. Sci. 48 (12) (2013) 2517–2530, https://doi.org/10.1111/maps.12223.
[24] D. Cellai, M.A. Carpenter, R.J. Kirpatrick, E.K.H Salje, M. Zhang, Thermally induced phase transition in Tridymite: an infrared spectroscopy study, Phys. Chem. Minerals 22 (1995) 50–60.
[25] A. Gendron-Badou, T. Coradin, J. Maquet, F. Fröhlich, J. Livage, Spectroscopic characterization of biogenic silica, J. Non-Cryst. Solids 316 (2013) 331–337, https://doi.org/10.1016/S0022-3093(02)01634-4.
[26] H.W. Marel van der, H. Beutelspacher, Atlas of Infrared Spectroscopy of Clay Minerals and their Admixtures, Elsevier, 1976.
[27] E. Mallard, Sur la lussatite, nouvelle variété minérale cristallisée de silice, Bull. Soc. Fran. Minéral 13 (2) (1890) 63–66 https://www.persee.fr/doc/bulmi_0366-3248_1890_num_13_2_2147.
[28] O.W. Flörke, H. Graetsch, B. Jones, Hydrothermal deposition of cristobalite, N. Jb. Miner. Mh., H 2 (1990) 81–95.
[29] A. Nukui, H. Nakazawa, M. Kao, Thermal changes in monoclinic tridymite, Amer Miner 63 (1978) 1252–1259.
[30] K. Kihara, Disorder and successive transitions in the tridymite forms of SiO_2, Phys. Chem. Minerals 22 (1995) 223–232.
[31] A.K.A. Pride, M.T. Dove, On the sequence of phase transitions in tridymite, Phys. Chem. Minerals 36 (1998) 171–179.
[32] H. Graetsch, Characterization of the high temperature modifications of incommensurate tridymite L3-T_o (MX-1) from 25 to 2050°C, Amer. Miner. (1998) 872–880.
[33] H. Graetsch, X-ray powder diffraction study on the modulated high temperature forms of SiO_2 tridymite between 110 and 220°C, Phys. Chem. Minerals 28 (2001) 313–321.
[34] PM Dove, J.D. Rimstidt, Silica-water interactions, in: P.J. Heany, C.T. Prewitt, G.V. Gibbs (Eds.), Silica physical behavior, geochemistry and materials applications, Rev. in Min. vol. 29, Miner, Soc. Amer. Washington, 1994, pp. 259–308.
[35] M. Sirarz, H. Handke, W. Mosgawa, Identification of silicooxygen rings in SiO_2 based on IR spectra, Spectroch. Acta Part A 56 (2000) 1819–1823, https://doi.org/10.1016/S1386-1425(00)00241-9.
[36] H. Graetsch, Structural characteristics of opaline and microcrystalline silica minerals, in: P.J. Heany, C.T. Prewitt, G.V. Gibbs (Eds.), Silica Physical Behavior, Geochemistry and Materials Applications, 1994, pp. 209–232 Rev. in Min. vol. 29, Miner. Soc. Amer. Washington.
[37] J. Willey, Silica-alumina interactions in sea water, Marine Chem. 3 (1975) 227–240, https://doi.org/10.1016/0304-4203(75)90005-5.
[38] D.J. Tobler, S. Shaw, J.G. Benning, Quantification of initial steps of nucleation and growth silica nanoparticles: An *in-situ* SAXS and DLS study, Geoch. Cosmoch. Acta 73 (2009) 5377–5693, https://doi.org/10.1016/j.gca.2009.06.002.
[39] M.J. Wilson, J.D. Russel, J.M. Tait, A new interpretation of the structure of α-cristobalite, Contr. Miner. Petr. 47 (1974) 1–6.
[40] L.G. Eversull, R.ER. Ferrell, Disordered silica with tridymite-like structure in he Twiggs clay, Amer. Min. 93 (2008) 565–572, https://doi.org/10.2138/am.2008.2603.